Biomaterials 34 (2013) 1204–1212

Contents lists available at SciVerse ScienceDirect

Biomaterials

journal homepage: www.elsevier.com/locate/biomaterials

Bioluminescence resonance energy transfer using luciferase-immobilized quantum dots for self-illuminated photodynamic therapy

Chia-Yen Hsu [a], Ching-Wen Chen [a], Hsiu-Ping Yu [a], Yan-Fu Lin [a], Ping-Shan Lai [a,b,*]

[a] Department of Chemistry, National Chung Hsing University, No. 250, Kuo-Kuang Rd., Taichung 402, Taiwan
[b] Center of Nanoscience and Nanotechnology, National Chung Hsing University, No. 250, Kuo-Kuang Rd., Taichung 402, Taiwan

ARTICLE INFO

Article history:
Received 30 July 2012
Accepted 21 August 2012
Available online 12 October 2012

Keywords:
Photodynamic therapy
Energy transfer
Bioluminescence
Illumination
In vivo

ABSTRACT

Photodynamic therapy (PDT) is an innovative method for cancer treatment that involves the administration of a photosensitizing agent followed by exposure to visible light. An appreciable amount of a particular light source is a key to activate photosensitizers in PDT. However, the external excitation light source is a problem for clinical application because of the limitation of tissue-penetrating properties. Additionally, the wavelength of laser emission should match the absorption wavelength of each photosensitizer for efficient generation of reactive oxygen species and cell killing. In this study, Renilla luciferase-immobilized quantum dots-655 (QD-RLuc8) was used for bioluminescence resonance energy transfer (BRET)-mediated PDT to resolve these problems. The bioluminescent QD-RLuc8 conjugate exhibits self-illumination at 655 nm after coelenterazine addition, which can activate the photosensitizer, Foscan®-loaded micelles for PDT. Our results show that BRET-mediated PDT by QD-RLuc8 plus coelenterazine (20 μg/mL) successfully generated reactive oxygen species (40.8%), killed ~ 50% A549 cells at 2 μg/mL equivalent Foscan® *in vitro* and significantly delayed tumor growth *in vivo* due to cell apoptosis under TUNEL analysis without obvious weight loss. Based on immunohistochemical observations, the proliferating cell nuclear antigen (PCNA)-negative area of tumor sections after BRET-mediated PDT was obviously increased compared to the PDT-untreated groups without an external light source. We conclude that this nanotechnology-based PDT possesses several clinical benefits, such as overcoming light penetration issues and treating deeper lesions that are intractable by PDT alone.

1. Introduction

Photodynamic therapy (PDT) utilizes a combination of photosensitizers and specific light sources for the treatment of various diseases. Following the activation of photosensitizers by illumination, reactive oxygen species (ROS) are generated by either hydrogen abstraction/electron transfer or energy transfer and subsequently destroy cancer cells [1]. Clinically, the primary side effect of PDT is skin photosensitivity, which is inconvenient for patients for several weeks [2]. In addition, the depth of light penetration required for photosensitizer activation is a major limitation for the wide application of PDT.

Nanotechnology-based drug delivery systems, such as polymer–drug conjugates [3,4], liposomes [5,6], nanoparticles [7,8], and polymeric micelles [9], are considered to be potentially improved hydrophobic drug delivery strategies that avoid the previously mentioned problems of photosensitizers. For example, hydrophobic photosensitizers tend to aggregate in aqueous solution, resulting in less photoactivation and less $^1O_2$ in solution, with a subsequent reduction in PDT efficacy in tumor cell destruction [10]. Nanocarriers provide a hydrophobic environment for photosensitizer encapsulation, and a significant reduction of skin photosensitivity of photosensitizers *in vivo* has been significantly observed [11–14]. However, only a few reports have mentioned the revolution of PDT with regard to needless of external light irradiation. Liu et al. reported that LaF_3:Tb^{3+}–porphyrin nanoparticles can be activated by X-ray irradiation, which can be promising for deep cancer treatment; however, no biological results were shown [15]. Quantum dots (QDs) have been of great interest to many researchers due to their unique optical properties and photochemical stability and thus can serve as better fluorescent imaging probes compared to common organic fluorophores [16–20]. In general, QDs emit photons following sustained excitation from an external light source. Recently, a new type of QD conjugate,

* Corresponding author. Center of Nanoscience and Nanotechnology, National Chung Hsing University, No. 250, Kuo-Kuang Rd., Taichung 402, Taiwan. Tel.: +886 4 22840411x428; fax: +886 4 22862547.
E-mail address: pslai@email.nchu.edu.tw (P.-S. Lai).

0142-9612/$ – see front matter © 2012 Elsevier Ltd. All rights reserved.
http://dx.doi.org/10.1016/j.biomaterials.2012.08.044

prepared by light-emitting Renilla luciferase 8 (RLuc8) and carboxylate-containing QDs, can emit light through bioluminescence resonance energy transfer (BRET) as previous report [21]. When the conjugates are exposed to the coelenterazine, the substrate of RLuc8, energy is released from the substrate and transferred to QDs via BRET, thereby emitting photons from QDs. These self-illuminating QDs can act as probes/sensors for biomedical applications [22–25].

In this study, the bioluminescent QD was employed as an internal light source for *meta*-tetra-hydroxyphenyl-chlorin (m-THPC, Foscan®)-mediated PDT; this concept of PDT is shown in Scheme 1. It is supposed that the wavelength-tunable QDs/luciferase can serve as a versatile light source for activation of specific photosensitizers and the internal emitted light in the body may overcome the limitation of light penetration for PDT.

2. Materials and methods

2.1. Preparation of RLuc8-immobilized quantum dots

RLuc8 was kindly provided by Professor Sanjiv Sam Gambhir (Stanford University), and the RLuc8-immobilized QDs (QD-RLuc8) were prepared as previously described [26]. Briefly, 1 pmol of carboxylate-containing quantum dots (QD655) was mixed with the coupling agent EDC (N-(3-dimethylaminopropyl)- N′-ethyl-carbodiimide hydrochloride, 4000 equivalents to QDs) and RLuc8 protein (40 equivalents to QDs) in phosphate buffer (pH 7.4) and incubated for 1 h at room temperature. Next, excessive EDC and protein (MW: 37 kDa) were removed through filtration with a Millipore's Amicon Ultra Centrifugal Filter (MWCO 100 K) and centrifuged at 2700 × *g* at 4 °C. The bioluminescence of the washed conjugates was measured using a fluorescence spectrophotometer (JASCO FP-6300, Tokyo, Japan), and mobility was determined using agarose gel electrophoresis. Approximately 1 μg coelenterazine was added to QD-RLuc8, and luminescence signals were collected without the excitation light. The conjugates were then separated using 1% agarose gel electrophoresis in 0.5 × TAE buffer at 100 V for 25 min. The particle size of QD-RLuc8 was analyzed by dynamic light scattering (DLS, Zetasizer Nano ZS, Malvern Instruments, Worcestershire, UK) and a JEOL 1400 transmission electron microscope (TEM, JEOL Ltd., Tokyo, Japan).

2.2. Culture conditions

Human lung adenocarcinoma epithelial A549 cells were grown in 75-T culture flasks in Dulbecco's Modified Eagle's Medium (DMEM) medium supplemented with 10% fetal bovine serum and and 1% penicillin–streptomycin–neomycin solution in a humidified atmosphere at 37 °C under 5% CO_2. The cells were subcultured 2–3 times per week with 0.25% trypsin-EDTA.

2.3. Cytotoxicity of QD-RLuc8 conjugate-mediated PDT

For cytotoxicity studies, A549 cells were seeded into 96-well plates at a density of 10,000 cells per well and cultured for 24 h. To determine the cytotoxicity of QD-RLuc8-mediated PDT, cells were incubated in media containing QDs-RLuc8 for 3 h. Next, Foscan®-loaded micelles (2 μg equivalent m-THPC per mL; m-F; m-THPC was obtained from Biolitec Pharma Ltd., Edinburgh, UK and m-THPC-loaded poly(2-ethyl-2-oxazoline)-*b*-poly(D,L-lactide) micelle was prepared as our previous report [13]) were added to the wells, and the plates were incubated in a humidified atmosphere at 37 °C under 5% CO_2. After 3 h of incubation, the cells were washed twice with phosphate buffered saline (PBS). The photodynamic process was stimulated by adding media containing coelenterazine (0.5–2 μg; 5–20 μg/mL) to the wells. After incubation for 24 h, cytotoxicity was determined using the MTT assay [27], and the results were read using a scanning multiwell plate reader at 570 nm (SpectraMax® M2e, Molecular Devices, Sunnyvale, USA).

2.4. Measurement of BRET-mediated ROS production

Intracellular ROS level in A549 cells treated was detected by staining treated with the fluorescent dye 2′7′-duchlorodihydrofluorscein diacetate (H_2DCFDA; Invitrogen, Carlsbad, CA, USA). Cells were treated with m-F (2 μg m-THPC per mL)/coelenterazine (2 μg per well, 20 μg/mL), QD-RLuc8 (1 pmol)/m-F or QD-RLuc8/m-F/coelenterazine at 37 °C for 24 h to evaluate the BRET-mediated PDT. The positive control cells were treated with 50 mM H_2O_2 at 37 °C for 30 min. Subsequently, the cells were washed with PBS and incubated with 10 μM H_2DCFDA for 1 h at 37 °C. ROS were measured by Leica SP5 confocal microscopy (Leica, Nussloch, Germany) using an excitation of 488 nm and an emission of 515–540 nm. Intracellular ROS generation caught by H_2DCFDA was also quantitatively measured by Accuri™ C6 flow cytometer (BD Accuri Cytometers, Ann Arbor, MI, USA).

2.5. Antitumor efficacy of QD-RLuc8 conjugate-mediated PDT

The *in vivo* experimental protocols were approved by the Institutional Animal Care and Use Committee of National Chung Hsing University (IACUC of NCHU). Female BALB/cAnN.Cg-*Foxn1*^{nu}/CrlNarl nude mice (4–5 weeks old, 20 ± 2 g) were obtained from the National Laboratory Animal Center (Taiwan). All of the mice were kept in an air-conditioned facility fitted with an artificial light–dark cycle and provided standard food and filtered water. The mice were acclimated to this environment for at least three days prior to subcutaneous injection in the right hindquarter with 10^7 A549 lung cancer cells that had been suspended in serum-free DMEM. Tumor sizes and body weights were measured every 3–4 days for the

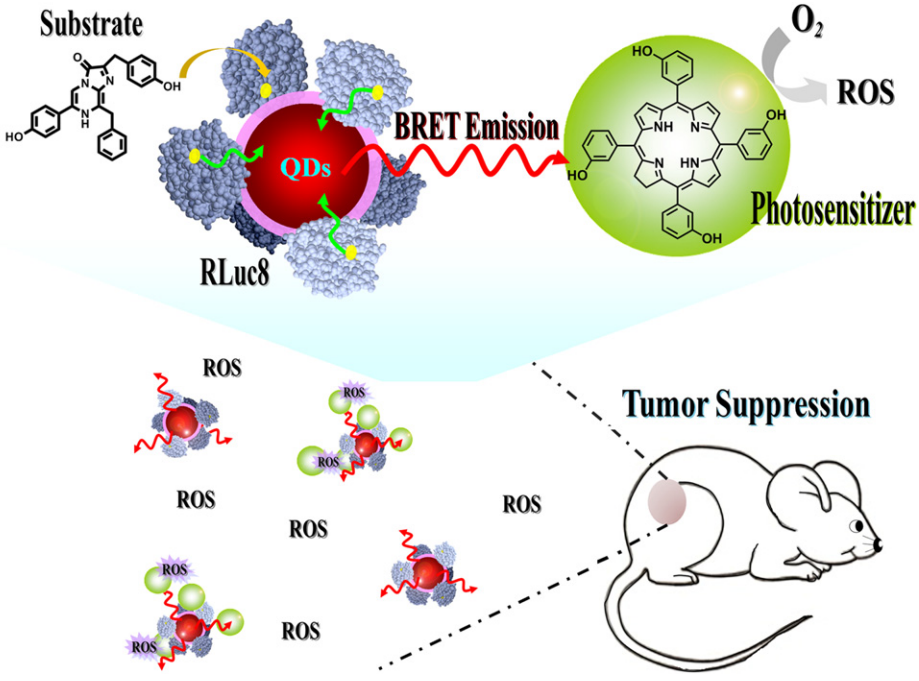

Scheme 1. Schematic representation of RLuc8-immobilized QDs-655 for BRET-based PDT.

duration of the experiment. Tumor volume was calculated as $1/2(4\pi/3)(L/2)(W/2)H$, where L is the length, W is the width, and H is the height of the tumor. Treatments were initiated when the tumors reached a volume of 50–100 mm^3 (day 0). Mice were randomized into four treatment groups ($n = 3$ per group). Animals were then treated with 0.1 mL PBS (control group), Foscan®-loaded micelles plus coelenterazine (m-F/coelenterazine group), QD-RLuc8 plus Foscan®-loaded micelles (QD-RLuc8/m-F group), or combination of QD-RLuc8, Foscan®-loaded micelles and coelenterazine (QD-RLuc8/m-F/coelenterazine group). PBS, m-F (0.3 mg/kg) or QD-RLuc8 (10 pmol/tumor) was first administrated by intratumor injection, followed by tail vein injection of 20 μg coelenterazine. The percentage of tumor growth inhibition (TGI%) was calculated from the relative tumor volume at day 20.

2.6. Necropsy and immunohistochemical analysis

Tumors were excised and weighed after 20 days of observation. For the immunohistochemical or hematoxylin and eosin (H&E) staining procedures, the tumor tissue was fixed in formalin and embedded in paraffin. Paraffin-embedded 2-μm tumor sections were analyzed by immunohistochemistry for proliferating cell nuclear antigen (PCNA) and CD31 (PECAM-1) expression. Briefly, sections were deparaffinized, rehydrated and incubated in 3% H_2O_2 to inhibit endogenous peroxidase activity. The sections were then incubated with diluted normal blocking serum to block nonspecific protein-binding sites and subsequently with primary antibodies against PCNA (PC10, 1:200, Dako, Denmark) or CD31 (rat anti-mouse, 1:50, Abcam, England). After being rinsed with ddH_2O, the tissue sections were incubated with the appropriate biotinylated secondary antibody for 30 min at room temperature. The avidin–biotin complexes were visualized with the 3,3′-diaminobenzidine tetrahydrochloride (DAB) chromogen. Sections were also counterstained with hematoxylin. Stained sections were monitored at low power (40×) and counted under high-power magnification (400×) using a light microscope (BX 50, OLYMPUS) equipped with a digital camera (DP 20, OLYMPUS). Cells that stained positive for PCNA or CD31 were counted under 400× magnification in at least five different fields. The proportions (%) of PCNA- or CD31-stained cells were quantified with Image Pro Plus software (Media Cybernetics Inc., Silver Spring, MD, USA).

2.7. TUNEL analysis of tumor sections

Cell apoptosis was analyzed by a terminal deoxynucleotidyl transferase dUTP nick end-labeling assay (TUNEL) assay using a Click-iT® TUNEL Alexa Fluor Imaging Assay Kit (Invitrogen, Carlsbad, CA, USA), and the experimental procedure was carried out according to the manufacturer's instructions. Briefly, 2 μm sections of tumors from mice in each treatment group were immersed in 0.25% Triton® X-100 PBS solution. After washing with PBS, slices were stained with TdT reaction cocktail for 90 min at 37 °C and washed with PBS. Next, Click-iT® reaction cocktail and Hoechst 33342 were used to stain the sections in the dark to label apoptotic cells and cellular DNA. After staining, Hoechst 33342 and Alexa Fluor® 488 fluorescence was observed by Leica SP5 confocal microscopy (Leica, Nussloch, Germany) using an excitation of 405 nm or 488 nm, respectively.

2.8. Statistical analysis

The treatment effects on the relative tumor volume were tested with a linear mixed model using the Bonferroni correction and presented as the estimated marginal means (EM means) and the corresponding 95% confidence interval (CI) of the tumor volume, with an adjustment for time effects. Statistical significance was set at least 0.05. Statistical analyses were performed using the SPSS 15.0 software package (SPSS Inc., Chicago, IL, USA).

3. Results

3.1. Characterization of QD-RLuc8 conjugates

QD-RLuc8 conjugates were synthesized via amide couplings between the QDs and a stabilized variant of RLuc8. The coupling reagent EDC was utilized to mediate amide bond formation between amino groups present on the surface of the protein and

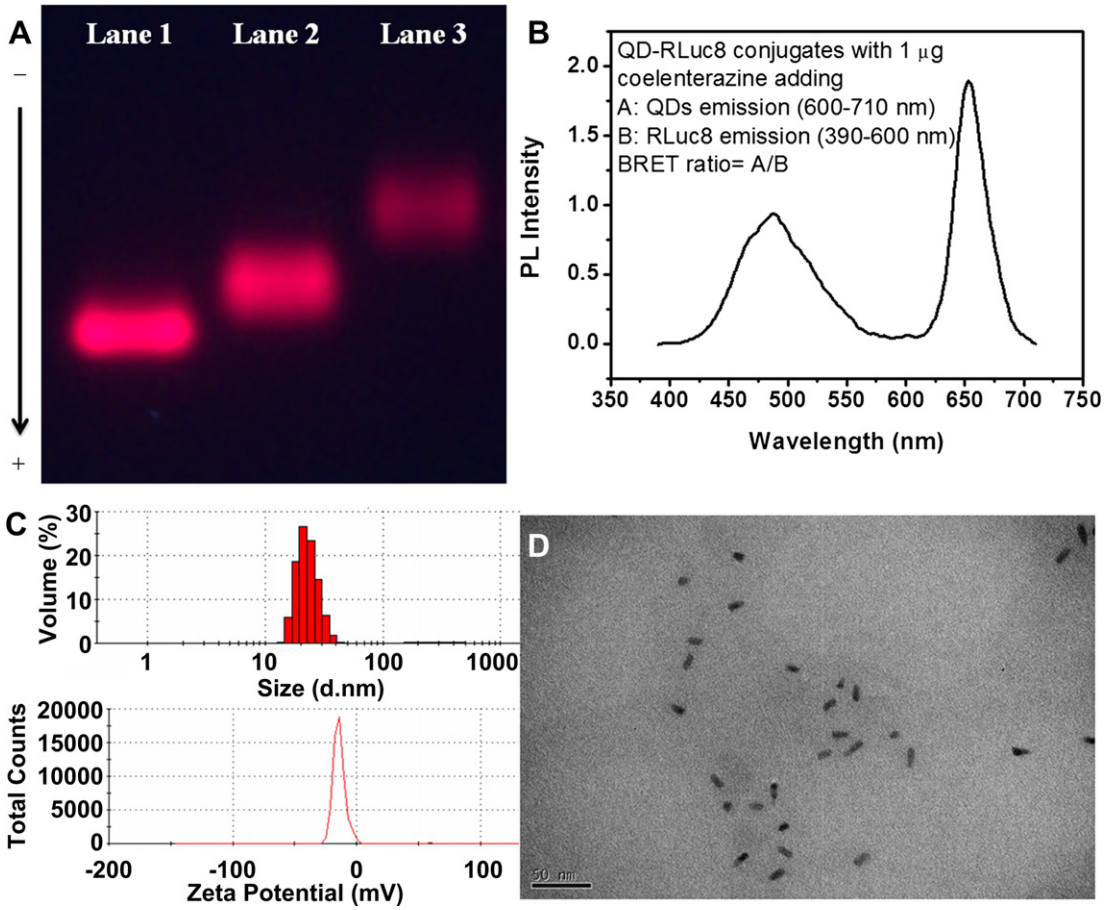

Fig. 1. Characterization of QD-RLuc8 conjugates. (A) Agarose gel electrophoretogram of components from the conjugation reaction. Lane 1, unconjugated QDs; lane 2, mixture of QDs and the coupling reagent EDC; lane 3, purified QD-RLuc8 conjugates. (B) Luminescence emission spectrum of QD-RLuc8 with coelenterazine (1 μg) adding. (C) Particle size and zeta potential of QD-RLuc8 measured by DLS. (D) Particle size and morphology of QD-RLuc8 observed by TEM. Scale bar: 50 nm.

the carboxylates of the QDs. As shown in Fig. 1A, significantly different levels of mobility were observed between conjugated (lane 3) and unconjugated QDs (mixture, lane 2; free QDs, lane 1) with agarose gel electrophoresis. Thus, RLuc8 was successfully immobilized onto QDs, as indicated by the change in the charge-to-surface area ratio of QDs [28]. In BRET, energy transfer is often presented as the BRET ratio, which is defined as the acceptor emission relative to the donor emission [26]; the larger the BRET ratio, the more efficient the energy transfer. Fig. 1B shows the emission spectrum of the self-illuminating QDs containing two peaks: one peak at 480 nm from RLuc8, and the other peak at 655 nm from the QDs. Area A is the integrated total emission (600–710 nm) from the QDs, and area B is the integrated total emission from RLuc8 (390–600 nm). The BRET efficiency is defined as the ratio of A to B [21] and the BRET ratio of our prepared QD-RLuc8 conjugate was approximately 0.92 with coelenterazine adding. The size of QD-RLuc8 was measured using DLS and TEM. Our DLS results showed that the particle size of the QD-RLuc8 conjugates was approximately 22 nm, with a zeta potential of approximately −12 mV (Fig. 1C); this result was consistent with particle size of cylindrical QD-RLuc8 observed by TEM (Fig. 1D). Clearly, the size of the QD-RLuc8 conjugates was slightly larger

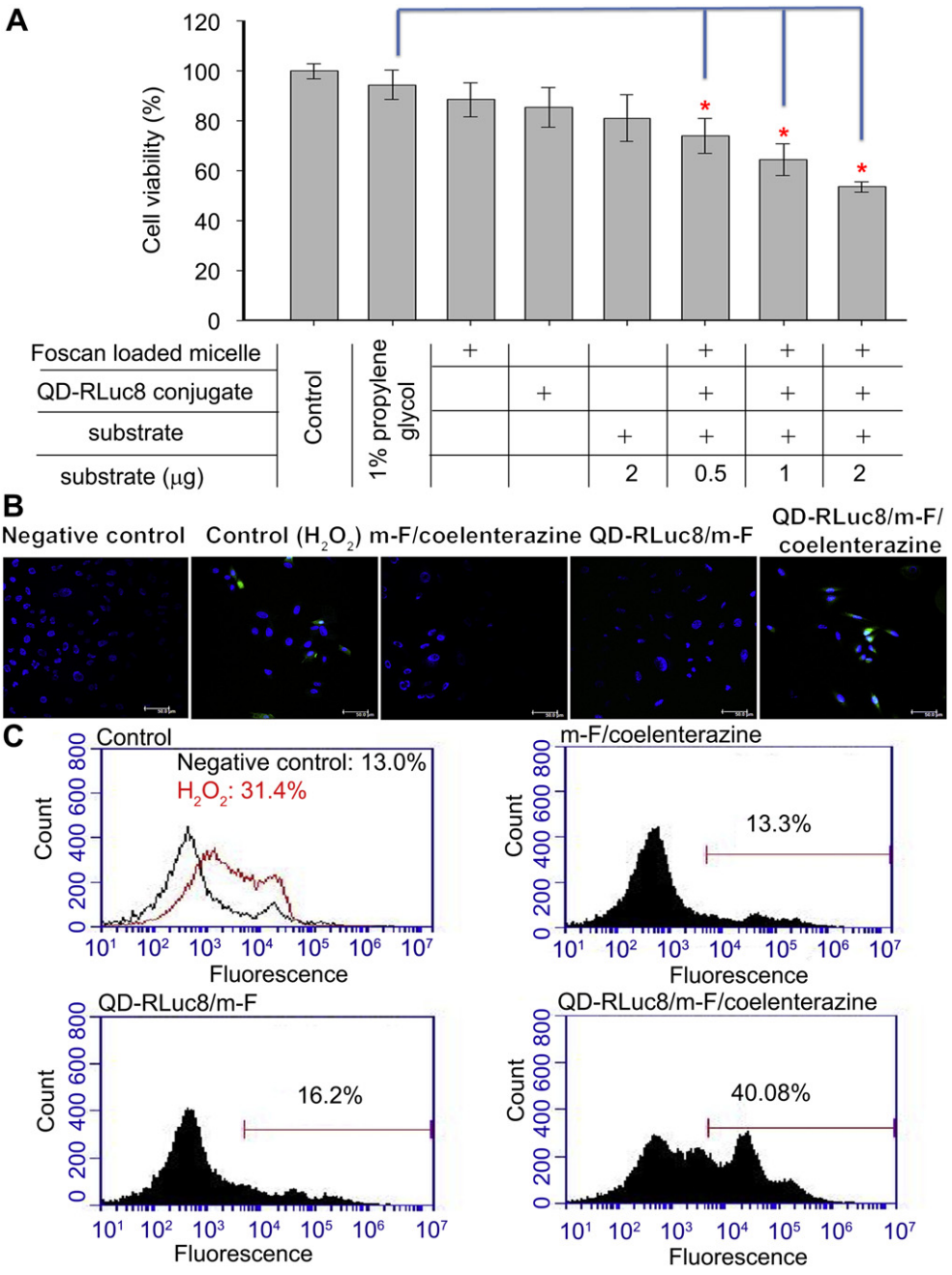

Fig. 2. (A) Cytotoxicity and ROS production following QD-RLuc8 conjugate-induced PDT. Cell viabilities of QD-RLuc8 conjugate-induced PDT. m-F (2 μg m-THPC equivalents/mL); QD-RLuc8 conjugate (1 pmol); coelenterazine (0.5–2 μg per well, 5–20 μg/mL). * indicates significant difference compared to the 1% propylene glycol group ($p < 0.05$). (B) ROS production of QD-RLuc8 conjugate-mediated PDT in A549 cells observed by confocal microscopy. Green: ROS indicator H_2DCFDA; blue, Hoechst 33342 (nuclei); scale bar, 50 μm. (C) Quantification of ROS of QD-RLuc8 conjugate-mediated PDT in A549 cells with H_2DCFDA staining measured by flow cytometry. (For interpretation of the references to color in this figure legend, the reader is referred to the web version of this article.)

than unconjugated QDs (approximately 17 nm) after RLuc8 immobilization.

3.2. Cytotoxicity and ROS production following QD-RLuc8 conjugate treatment with or without photosensitizer/substrate co-incubation

Fig. 2A shows the cytotoxicities of combination or alone treatment of QD-RLuc8, coelenterazine or m-F in A549 cells. The cytotoxicity of QD-RLuc8 plus m-F was clearly enhanced by increasing the concentration of coelenterazine (0.5–2 μg; 5–20 μg/mL), whereas no significant cell death was observed after QD-RLuc8 conjugate, m-F or substrate treated alone. Approximately 50% cells were killed when the concentration of coelenterazine was increased to 2 μg per well (20 μg/mL). This enhancement of cytotoxicity was supposed to the coelenterazine catalyzed by QD-RLuc8 conjugates, which stimulated the BRET process, emitted 655 nm photons and thereby activated the photosensitizer for ROS production. Thus, this endogenous light production strategy is potential for cell killing. Intracellular ROS generation in A549 cells was evaluated by H_2DCFDA staining with confocal microscopy and flow cytometry. As shown in Fig. 2B and C, the green fluorescence signal of ROS generation was detected in A549 cells treated with either 50 mM H_2O_2 (positive control: 31.1%) or QD-RLuc8/m-F/coelenterazine combination (40.8%) but was not significantly detected by confocal microscopy or flow cytometey in the negative control, QD-RLuc8 conjugate or substrate groups (13.0%, 13.3% or 16.2%, respectively). Thus, we showed that PDT can be processed without an external light source and that the endogenous BRET process can potentially activate a photosensitizer, producing ROS and therefore resulting in cell death.

3.3. Antitumor efficacy of BRET-based PDT

To evaluate the effects of BRET-PDT using QD-RLuc8 conjugates on *in vivo* antitumor efficacy, mice were treated with QD-RLuc8 conjugate, the photosensitizer, the substrate or various combinations of these, and the antitumor effect of these treatments was evaluated by measuring tumor growth rates (Fig. 3A). To prove that endogenous BRET induced PDT, we directly injected QD-RLuc8 and m-F into tumors and then treated animals with coelenterazine via intravenous injection. There is no significant body weight loss in each treated groups during the observation time (Fig. S1). In general, the relative tumor volumes in each treatment group increased from day 3 to day 20 after treatment; the relative tumor volumes were highest in the PBS control, m-F/coelenterazine, and QD-RLuc8/m-F groups. On day 20, the mean relative tumor volumes of PDT-untreated animals (PBS control, m-F/coelenterazine and QD-RLuc8/m-F groups) were approximately 4.5–6 times

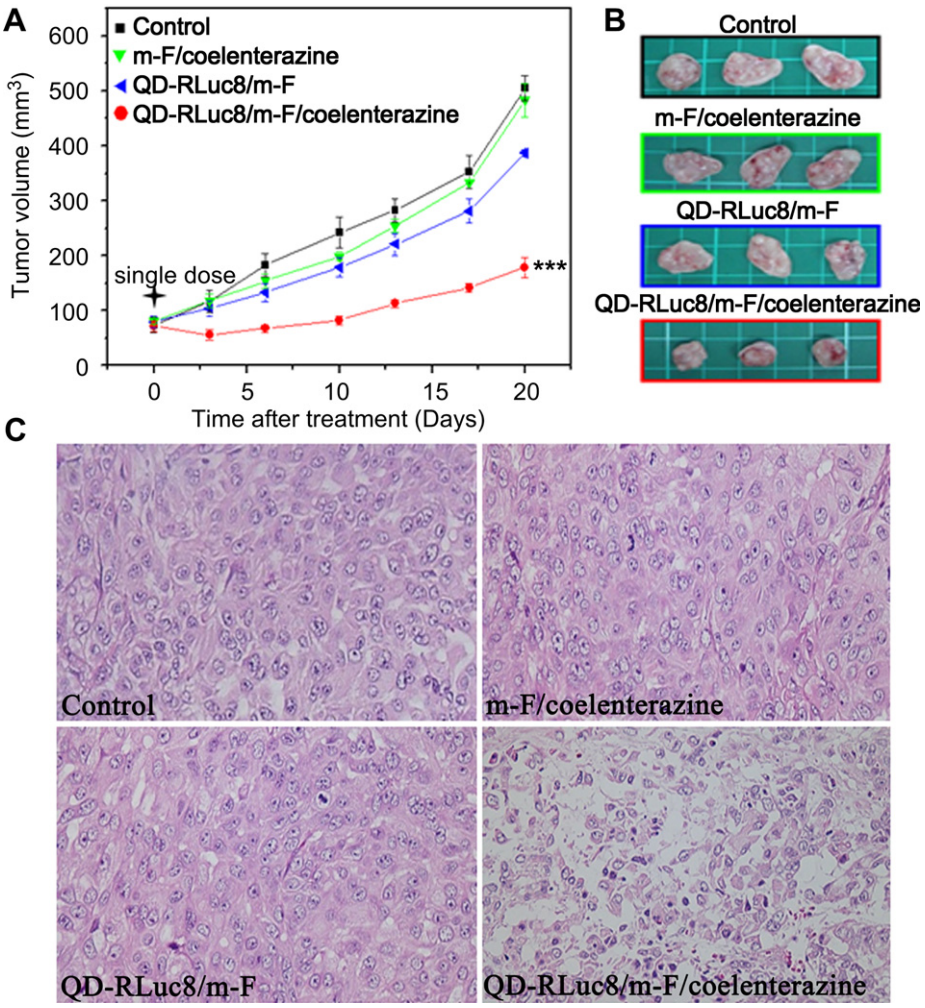

Fig. 3. Relative tumor growth curves and structural characteristics of tumors from different treatment groups. (A) Relative growth curves of A549 tumors after various treatments. m-F (0.3 mg m-THPC equivalents/kg); QD-RLuc8 conjugate (10 pmol); coelenterazine (20 μg). *** indicates significant differences compared to the control group ($p < 0.0001$) (B) Hematoxylin- and eosin-stained histological sections of tumors.

higher than the initial volumes. In the QD-RLuc8/m-F/coelenterazine group, the tumor growth profile was significantly delayed compared to the PDT-untreated groups (control, m-F/coelenterazine or QD-RLuc8/coelenterazine groups; $p < 0.0001$). Isolated tumors were also observed after the mice from each group were sacrificed (Fig. 3B). The isolated tumor sizes of the PDT treated group (QD-RLuc8/m-F/coelenterazine) was significantly smaller than those of the m-F/coelenterazine (TGI % = 4.2) or QD-RLuc8/coelenterazine (TGI % = 23.3) groups. This result indicates that BRET-based PDT can be stimulated using QD-RLuc8/m-F/coelenterazine co-treatment although the optimized conditions for BRET-mediated PDT are needed to further investigation.

3.4. Effect of PDT treatment on cellular proliferation in the tumor environment

To evaluate the effects of QD-RLuc8-mediated PDT, tumor specimens from mice sacrificed on day 20 were fixed, embedded, sectioned and stained for H&E, PCNA and CD31 observation. As shown in Fig. 3C, H&E-stained tissue sections showed differences in tissue morphology between the treatment groups; prominent apoptosis was clearly apparent in the BRET-PDT group, and almost no effects were observed in PDT-untreated groups. Cell proliferation maker PCNA, a nuclear protein synthesized in the late G1 and S phases of the cell cycle, was assessed for immunohistochemical analysis. As shown in Fig. 4A, mice treated with m-F/coelenterazine or QD-RLuc8/m-F displayed high proportions of PCNA-positive cells (87.4 ± 1.6% and 75.2 ± 2%, respectively; Fig. 4A), whereas control groups had 92.2 ± 1.4% PCNA-positive cells (Fig. 4A). In contrast, tumors from mice treated with BRET-mediated PDT exhibited significantly decreased cell proliferation, as detected by PCNA expression (27.1 ± 2.6%, Fig. 4A), compared with the non-PDT-treated groups. Therefore, BRET-mediated PDT stimulated by QD-RLuc8/coelenterazine plus m-F can efficiently reduce tumor cell proliferation in an A549 xenograft model after intratumor injection.

3.5. Effects of BRET-mediated PDT on microvessel density

PDT can cause the massive destruction of tumor cells or damage to the tumor microvasculature and vessel occlusion. To investigate the vascular effects of BRET-mediated PDT on tumor angiogenesis *in vivo*, tumor sections were analyzed for CD31 expression, and the results are shown in Fig. 4B. In the absence of PDT, tumors exhibited high microvessel density (MVD, control, 9.4 ± 0.8%; m-F/coelenterazine, 8.1 ± 0.5%; QD-Luc8/m-F, 6.8 ± 0.3%; Fig. 4B); however, tumors treated with QD-RLuc8-mediated BRET-PDT had significantly lower degrees of vascularization (Fig. 4B: 2.5 ± 0.3%; $p < 0.01$). This finding indicates that BRET-based PDT not only significantly reduced cell proliferation but also decreased the vascular density compared with coelenterazine plus m-F or QD-RLuc8 alone, resulting in tumor growth suppression.

3.6. Effects of BRET-mediated PDT on cell apoptosis

The PDT antitumor effect may either cause vascular impairment, resulting in deficient nutrient supply, or increase the amount of oxidation species, which directly induce tumor cell apoptosis. Thus, the frequency of apoptotic cells in paraffin-embedded A549 tumor sections from each group was analyzed by a TUNEL (terminal deoxynucleotidyl transferase [TdT]-mediated deoxyuridine-triphosphate [dUTP] nick end-labeling) assay. As shown in Fig. 5, the colocalization of nuclei (Hoechst staining, shown in red) and TUNEL-positive apoptotic cells (green) in tumor sections were

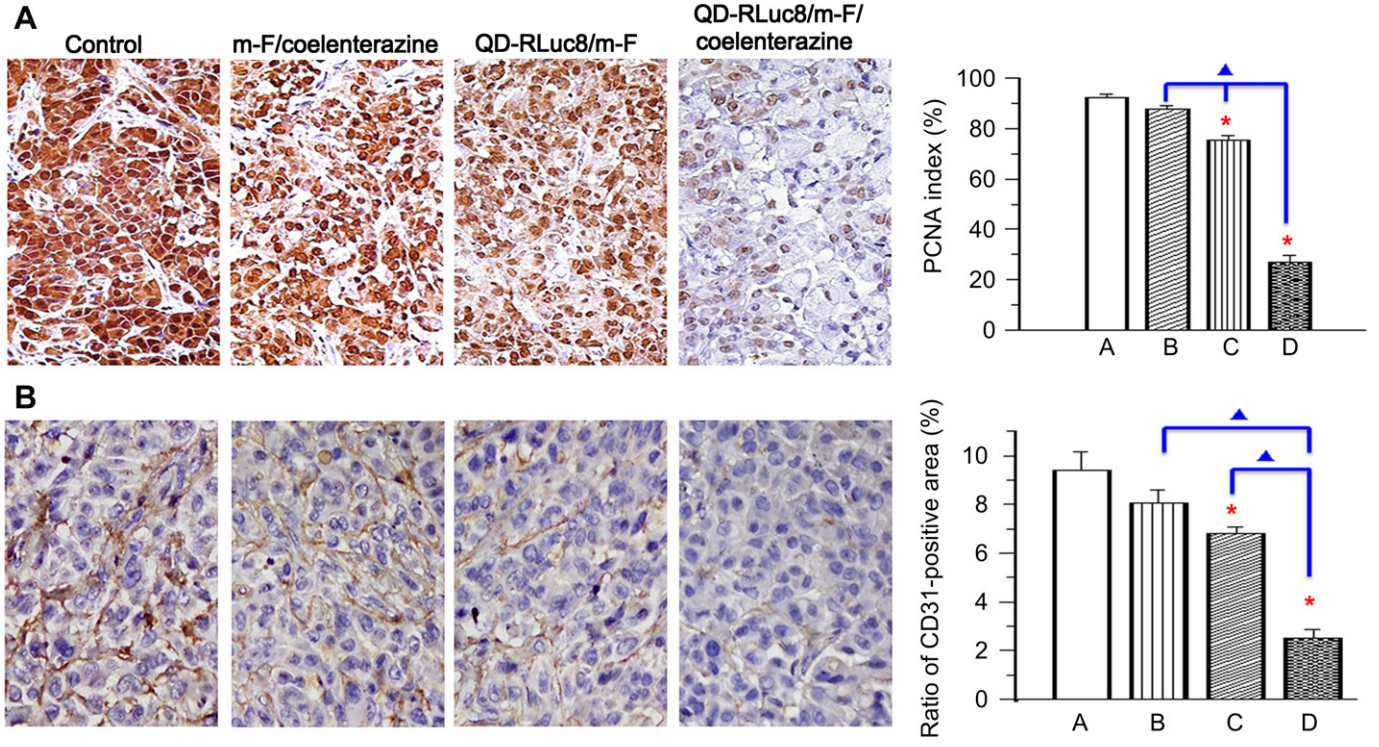

Fig. 4. Immunohistochemical analysis of (A) PCNA and (B) CD31 in A549 xenografts from tumors treated with the photosensitizer, QD-RLuc8, substrate or a combination for PDT. Cellular proliferation was quantified by assessing the number of PCNA-positive cells and microvessel density was quantified by assessing the number of CD31-positive cells. A: control group; B: m-F/coelenterazine; C: QD-RLuc8/m-F; D: QD-RLuc8/m-F/coelenterazine. * indicates significant differences compared to the control group ($p < 0.001$). ▲ indicates the paired comparisons with significant differences ($p < 0.0001$).

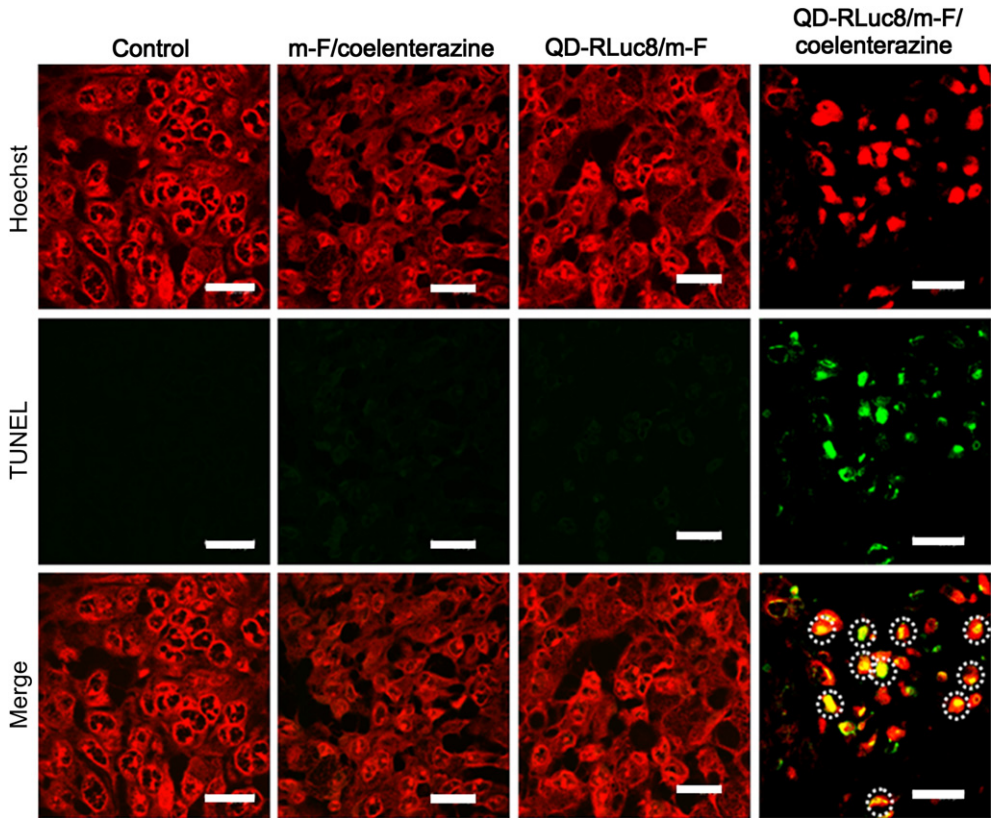

Fig. 5. Apoptotic analysis of the A549 tumors from different treated groups by TUNEL staining under confocal microscopy observation. Hoechst 33342 was used for nuclei staining and observed with excitation 405 nm (shown in red). TUNEL staining with excitation 488 nm was utilized to visualize apoptotic cells. Scale bar: 20 μm. (For interpretation of the references to color in this figure legend, the reader is referred to the web version of this article.)

significantly increased in the group with QD-RLuc8-mediated BRET-PDT whereas no significant TUNEL fluorescence was observed in m-F/coelenterazine or QD-RLuc8/m-F group. This result strongly indicates that cell apoptosis was only stimulated by QD-RLuc8-mediated BRET-PDT, which inhibited tumor growth in the A549 xenograft animal model.

4. Discussion

PDT is a clinical method used to treat a wide range of malignant cancers. This treatment procedure consists of the two following steps: the administration of a photosensitive drug and exposure of the drug to visible light to activate the agent [29]. However, the limitation of PDT is external excitation light source application because of its tissue-penetrating properties. Additionally, laser (ex. light source) and photosensitizer should be paired because the emission of laser has to match the wavelength absorption of photosensitizer for its efficient activation. Therefore, we improved upon the PDT method by using QD-RLuc8 for BRET-based PDT to resolve these problems (Scheme 1).

Similar concepts without external light sources for PDT have been previously used with luciferase-mediated molecular flashlights to activate photosensitizers for antiviral study and mammalian cell killing. Carpenter et al. reported that the natural photosensitizer hypericin can be effectively activated by bioluminescence from the *Photinus pyralis* luciferin/luciferase system for efficient PDT against equine infectious anemia virus [30]. Theodossiou et al. transfected the firefly luciferase gene into mouse embryo fibroblast NIH 3T3 cells and found that the NIH 3T3-luc$^+$ cells can be killed by Rose Bengal and luciferin co-treatment *in vitro* [31]. A similar study was also performed by Schipper et al. [32]; however, no obvious cytotoxicity by firefly D-luciferin bioluminescence-mediated PDT was observed in non-transgenic or transgenic tumor cells, although the bioiluminescent photon output from the firefly luciferase gene-transfected neuro 2a neuroblastoma cells (N2afLuc) was approximately 40-fold higher than that of the NIH 3T3-luc$^+$ cells reported by Theodossiou et al. It has been suggested that the genotype of NIH 3T3-luc$^+$ cells in the Theodossiou et al. report may contain an unknown mutation that resulted in transgenic cells that were more sensitive to PDT. Importantly, it was assumed that both high-level bioluminescent light production and photosensitizers restricted to the same cellular compartment may reveal an observable PDT effect [32]. Therefore, shortening the distance between the intracellular light source and photosensitizers may improve the efficacy of PDT when we use the molecular flashlight from the luciferin/luciferase system as an internal light source for photosensitizer activation. Foscan® is one of the most available and effective photosensitizers in clinical use, and it possesses a high extinction coefficient in the red part of the spectrum (652 nm) that allows deeper lesions to be treated and high singlet oxygen quantum yields at lower concentrations of drug, which therefore decreases toxicity toward normal tissues [2]. However, free Foscan® drug accumulates in the endoplasmic reticulum and Golgi apparatus, as shown in human breast adenocarcinoma cells (MCF-7) and A549 cells [33,34]. In contrast to free Foscan®, nanotechnology-based drug delivery systems, such as photosensitizer-loaded micelles or liposomes, have been shown in previous studies to most likely be sequestered in acidic organelles, such as the endo/lysosome [13,34]. Further, micellar Foscan® encapsulation has been shown to have reduced skin

photosensitivity *in vivo* compared with free Foscan® [13,14]. Typically, nanocrystals of QDs are taken up by live cells via endocytosis and also trapped in acidic endosomes, except for those with specific endosomal-disrupting surface modifications [35,36]. Thus, we supposed that nano-sized endogenous light sources of QD-RLuc8 may also be taken up via endocytosis and may therefore increase the encounter probability and decrease the distance between photosensitizer and endogenous light sources in cellular organelles. Therefore, the ability to use BRET-mediated PDT was evaluated by shortening the distance between light source and photosensitizer via light-controllable QDs (QD-RLuc8) and micellar photosensitizer (m-F) in this study. Our *in vitro* data showed that QD-RLuc8 combined with a micellar photosensitizer enhanced the cytotoxicity of A549 cells by increasing the concentration of coelenterazine (Fig. 2A). This BRET-mediated PDT can also be observed in HeLa cells (Fig. S2). However, the co-treatment of QD-RLuc8 and free Foscan® did not significantly decrease the cell viability in A549 cells (data now shown).

The *in vivo* treatment of mice with QD-RLuc8, m-F and endogenous irradiation activated by coelenterazine successfully showed tumor destruction activity with proliferation factor PCNA and microvessel densities decreasing. Similar results were observed micellar photosensitizer-mediated PDT *in vivo* [12,14,37]. The mechanism of the anti-tumor effect mediated by PDT involves a variety of events. The photosensitizer activation by light irradiation produces energy transfer and a local chemical effect, such as the generation of ROS. These devastating reactions will kill cells through apoptosis or necrosis [38]. The new concept of BRET-mediated PDT revealed efficient intracellular ROS generation due to the activation of the photosensitizer Foscan® by coelenterazine catalyzed by QD-RLuc8 (Fig. 2B and C), thereby increasing TUNEL-positive apoptotic cells in BRET-mediated PDT group (Fig. 5). The PDT efficacy of BRET-mediated PDT compared with PDT with external light irradiation was also evaluated *in vitro*. At the same concentration of m-F (2 μg m-THPC equivalents per mL), PDT with endogenous irradiation strategy yield similar efficacy compared to that with 0.6–0.8 J/cm^2 external light irradiation in A549 cells (Fig. S3). The relationship between the light dose required to induce PDT and cell death has also been explored in previous studies [39,40]. Although apoptosis was expected to predominate cell death post-PDT treatment, necrosis also occurred at higher light doses [41]. In this work, the endogenous irradiation strategy could output an approximate 0.6–0.8 J/cm^2 light dose during treatment; this low light dose-PDT may prevent necrosis and decrease undesired inflammation relative to PDT with external light irradiation.

Fig. 6. The future speculation about BRET-mediated PDT with versatile and wavelength-tunable QDs for present clinical approved, clinical trial or preclinical trial photosensitizers.

It is known that the versatile QDs can emit different wavelengths of irradiation based on its particle size. This wavelength-tunable photoluminescence property of QDs are speculated that can be potentially utilized to match the excited wavelength of present clinical approved, in clinical trial or in preclinical trial photosensitizes (Fig. 6) although only Foscan®/QD655 nm pair was evaluated in this study. In addition, the nanotoxicity of CdSe QDs used in this study is needed to be evaluated for further applications. This limitation might be overcome with the increase in new materials with wavelength-tunable photoluminescence, such as silicon dots [42] or carbon dots [43]. Taken together, BRET-mediated PDT can be processed without an external light source, which may improve the efficacy in deeper tumor areas. The delivery systems containing illumination and photosensitizers in one nanoparticle, and the conditions for optimized BRET-mediated PDT are currently being developed at our lab.

5. Conclusions

Light penetration is currently a limitation for clinical PDT. In this study, we demonstrated that BRET-mediated PDT may improve this intractability. The photochemical process of photosensitizers was stimulated by 655 nm emission from QD-RLuc8/coelenterazine system. Both *in vitro* and *in vivo* results revealed the potential for BRET-mediated PDT using QD-RLuc8 conjugates without an external light source for cancer therapy. This nanotechnology-based PDT possesses several clinical benefits, such as overcoming light penetration issues and treating deeper lesions that are intractable by PDT alone.

Acknowledgments

We thank the National Science Council of Taiwan for their financial support of this work (NSC 98-2213-M-005-007-MY2). We are also grateful to Professor Sanjiv Sam Gambhir and Professor Jianghong Rao for the RLuc8 support in this study.

Appendix A. Supplementary data

Supplementary data related to this article can be found, in the online version, at http://dx.doi.org/10.1016/j.biomaterials.2012.08.044.

References

[1] Dolmans DE, Fukumura D, Jain RK. Photodynamic therapy for cancer. Nat Rev Cancer 2003;3:380–7.
[2] MacDonald IJ, Dougherty TJ. Basic principles of photodynamic therapy. J Porphyr Phthalocyanines 2001;5:105–29.
[3] Hsu CY, Nieh MP, Lai PS. Facile self-assembly of porphyrin-embedded polymeric vesicles for theranostic applications. Chem Comm 2012;48:9343–5.
[4] Lai PS, Lou PJ, Peng CL, Pai CL, Yen WN, Huang MY, et al. Doxorubicin delivery by polyamidoamine dendrimer conjugation and photochemical internalization for cancer therapy. J Control Release 2007;122:39–46.
[5] Takeuchi Y, Ichikawa K, Yonezawa S, Kurohane K, Koishi T, Nango M, et al. Intracellular target for photo sensitization in cancer antiangiogenic photodynamic therapy mediated by polycation liposome. J Control Release 2004;97:231–40.
[6] Bovis MJ, Woodhams JH, Loizidou M, Schegelmann D, Bown SG, MacRobert AJ. Improved in vivo delivery of m-THPC via pegylated liposomes for use in photodynamic therapy. J Control Release 2012;157:196–205.
[7] Baba K, Pudavar HE, Roy I, Ohulchanskyy TY, Chen YH, Pandey RK, et al. New method for delivering a hydrophobic drug for photodynamic therapy using pure nanocrystal form of the drug. Mol Pharmaceutics 2007;4:289–97.
[8] Shieh MJ, Hsu CY, Huang LY, Chen HY, Huang FH, Lai PS. Reversal of doxorubicin-resistance by multifunctional nanoparticles in MCF-7/ADR cells. J Control Release 2011;152:418–25.

[9] Jang WD, Nakagishi Y, Nishiyama N, Kawauchi S, Morimoto Y, Kikuchi M, et al. Polyion complex micelles for photodynamic therapy: incorporation of dendritic photosensitizer excitable at long wavelength relevant to improved tissue-penetrating property. J Control Release 2006;113:73–9.
[10] Redmond RW, Land EJ, Truscott TG. Aggregation effects on the photophysical properties of porphyrins in relation to mechanisms involved in photodynamic therapy. Adv Exp Med Biol 1985;193:293–302.
[11] Nishiyama N, Nakagishi Y, Morimoto Y, Lai PS, Miyazaki K, Urano K, et al. Enhanced photodynamic cancer treatment by supramolecular nanocarriers charged with dendrimer phthalocyanine. J Control Release 2009; 133:245–51.
[12] Peng CL, Lai PS, Lin FH, Wu SYH, Shieh MJ. Dual chemotherapy and photodynamic therapy in an HT-29 human colon cancer xenograft model using SN-38-loaded chlorin-core star block copolymer micelles. Biomaterials 2009;30: 3614–25.
[13] Shieh MJ, Peng CL, Chiang WL, Wang CH, Hsu CY, Wang SJJ, et al. Reduced skin photosensitivity with meta-tetra(hydroxyphenyl) chlorin-loaded micelles based on a poly (2-ethyl-2-oxazoline)-b-poly (D, L-lactide) diblock copolymer in vivo. Mol Pharmaceutics 2010;7:1244–53.
[14] Syu WJ, Yu HP, Hsu CY, Rajan YC, Hsu YH, Chang YC, et al. Improved photodynamic cancer treatment by folate-conjugated polymeric micelles in KB xenografted animal model. Small 2012;8:2060–9.
[15] Liu YF, Chen W, Wang SP, Joly AG. Investigation of water-soluble x-ray luminescence nanoparticles for photodynamic activation. Appl Phys Lett 2008;92:043901.
[16] Koshman YE, Waters SB, Walker LA, Los T, de Tombe P, Goldspink PH, et al. Delivery and visualization of proteins conjugated to quantum dots in cardiac myocytes. J Mol Cell Cardiol 2008;45:853–6.
[17] Murcia MJ, Minner DE, Mustata GM, Ritchie K, Naumann CA. Design of quantum dot-conjugated lipids for long-term, high-speed tracking experiments on cell surfaces. J Am Chem Soc 2008;130:15054–62.
[18] Zhang Y, So MK, Rao JH. Protease-modulated cellular uptake of quantum dots. Nano Lett 2006;6:1988–92.
[19] Chen XC, Deng YL, Lin Y, Pang DW, Qing H, Qu F, et al. Quantum dot-labeled aptamer nanoprobes specifically targeting glioma cells. Nanotechnology 2008;19.
[20] Michalet X, Pinaud FF, Bentolila LA, Tsay JM, Doose S, Li JJ, et al. Quantum dots for live cells, in vivo imaging, and diagnostics. Science 2005;307: 538–44.
[21] So MK, Xu CJ, Loening AM, Gambhir SS, Rao JH. Self-illuminating quantum dot conjugates for in vivo imaging. Nat Biotechnol 2006;24:339–43.
[22] Du J, Yu C, Pan D, Li J, Chen W, Yan M, et al. Quantum-dot-decorated robust transductable bioluminescent nanocapsules. J Am Chem Soc 2010;132:12780–1.
[23] Rao J, Dragulescu-Andrasi A, Yao H. Fluorescence imaging in vivo: recent advances. Curr Opin Biotechnol 2007;18:17–25.
[24] Xia Z, Rao J. Biosensing and imaging based on bioluminescence resonance energy transfer. Curr Opin Biotechnol 2009;20:37–44.
[25] Yao HQ, Zhang Y, Xiao F, Xia ZY, Rao JH. Quantum dot/bioluminescence resonance energy transfer based highly sensitive detection of proteases. Angew Chem Int Ed 2007;46:4346–9.
[26] So MK, Loening AM, Gambhir SS, Rao JH. Creating self-illuminating quantum dot conjugates. Nat Protoc 2006;1:1160–4.
[27] Mosmann T. Rapid colorimetric assay for cellular growth and survival - applicarion to proliferation and cyto-toxicity assays. J Immunol Methods 1983;65:55–63.
[28] Kim JH, Chaudhary S, Ozkan M. Multicolour hybrid nanoprobes of molecular beacon conjugated quantum dots: FRET and gel electrophoresis assisted target DNA detection. Nanotechnology 2007;18.
[29] Chen J, Keltner L, Christophersen J, Zheng F, Krouse M, Singhal A, et al. New technology for deep light distribution in tissue for phototherapy. Cancer J 2002;8:154–63.
[30] Carpenter S, Fehr MJ, Kraus GA, Petrich JW. Chemiluminescent activation of the antiviral activity of hypericin: a molecular flashlight. Proc Natl Acad Sci 1994;91:12273–7.
[31] Theodossiou T, Hothersall JS, Woods EA, Okkenhaug K, Jacobson J, MacRobert AJ. Firefly luciferin-activated Rose Bengal: in vitro photodynamic therapy by intracellular chemiluminescence in transgenic NIH 3T3 cells. Cancer Res 2003;63:1818–21.
[32] Schipper M, Patel M, Gambhir S. Evaluation of firefly luciferase bioluminescence mediated photodynamic toxicity in cancer cells. Mol Imaging Biol 2006; 8:218–25.
[33] Teiten MH, Bezdetnaya L, Morliere P, Santus R, Guillemin F. Endoplasmic reticulum and golgi apparatus are the preferential sites of Foscan® localisation in cultured tumour cells. Br J Cancer 2003;88:146–52.
[34] Compagnin C, Moret F, Celotti L, Miotto G, Woodhams JH, MacRobert AJ, et al. Meta-tetra(hydroxyphenyl)chlorin-loaded liposomes sterically stabilised with poly(ethylene glycol) of different length and density: characterisation, in vitro cellular uptake and phototoxicity. Photochem Photobiol Sci 2011;10:1751–9.
[35] Lagerholm BC, Wang M, Ernst LA, Ly DH, Liu H, Bruchez MP, et al. Multicolor coding of cells with cationic peptide coated quantum dots. Nano Lett 2004;4: 2019–22.
[36] Bayles AR, Chahal HS, Chahal DS, Goldbeck CP, Cohen BE, Helms BA. Rapid cytosolic delivery of luminescent nanocrystals in live cells with endosome-disrupting polymer colloids. Nano Lett 2010;10:4086–92.
[37] Lu HL, Syu WJ, Nishiyama N, Kataoka K, Lai PS. Dendrimer phthalocyanine-encapsulated polymeric micelle-mediated photochemical internalization extends the efficacy of photodynamic therapy and overcomes the drug-resistance in vivo. J Control Release 2011;155:458–64.
[38] Luksiene Z. Photodynamic therapy: mechanism of action and ways to improve the efficiency of treatment. Medicina (Kaunas) 2003;39:1137–50.
[39] Kamuhabwa AR, Agostinis PM, D'Hallewin M-A, Baert L, De Witte PAM. Cellular photodestruction induced by hypericin in AY-27 rat bladder carcinoma cells. Photochem Photobiol 2001;74:126–32.
[40] Wyld L, Reed MW, Brown NJ. Differential cell death response to photodynamic therapy is dependent on dose and cell type. Br J Cancer 2001;84:1384–6.
[41] Luo Y, Kessel D. Initiation of apoptosis versus necrosis by photodynamic therapy with chloroaluminum phthalocyanine. Photochem Photobiol 1997; 66:479–83.
[42] Kang Z, Liu Y, Tsang CHA, Ma DDD, Fan X, Wong NB, et al. Water-soluble silicon quantum dots with wavelength-tunable photoluminescence. Adv Mater 2009;21:661–4.
[43] Sun YP, Zhou B, Lin Y, Wang W, Fernando KAS, Pathak P, et al. Quantum-sized carbon dots for bright and colorful photoluminescence. J Am Chem Soc 2006; 128:7756–7.